ELSEVIER

Nuclear Engineering and Design 195 (2000) 1–11

Nuclear Engineering and Design

www.elsevier.com/locate/nucengdes

# Ultimate analysis of BWR Mark III reinforced concrete containment subjected to internal pressure

Hsuan-Teh Hu *, Jiin-Iuan Liang

*Department of Civil Engineering, National Cheng Kung University, 1 University Road, Tainan, Taiwan 701, ROC.*

Accepted 15 June 1999

**Abstract**

Numerical analyses are carried out by using the ABAQUS finite element program to predict the ultimate pressure capacity and the failure mode of the BWR Mark III reinforced concrete containment at Kuosheng Nuclear Power Plant, Taiwan, R.O.C. Material nonlinearity such as concrete cracking, tension stiffening, shear retention, concrete plasticity, yielding of reinforcing steel, yielding of liner plate and degradation of material properties as a result of high temperature effects are all simulated with proper constitutive models. Geometric nonlinearity as a result of finite deformation has also been considered. The results of the analysis show that when the reinforced concrete containment fails, extensive cracks take place at the apex of the dome, the intersection of the dome and the cylinder and the lower part of cylinder where there is a discontinuity in the thickness of the containment. In addition, the ultimate pressure capacity of the containment is 23.9 psi and is about 59% higher than the design pressure 15 psi. 

## 1. Introduction

Since the accident at Three Mile Island nuclear plant in 1979, it has become necessary to perform failure analysis and calculate the ultimate pressure capability of the nuclear reactor containment for the safety assessment of nuclear power plants (U.S. Nuclear Regulatory Commission, 1987; Amin et al., 1993; Boeck, 1993). The containment structures in service at Taiwan, ROC were built in the late 1970s or early 1980s. Since then, nonlinear material constitutive models and nonlinear finite element solution techniques have been continuously and successfully developed (ASCE, 1982; Chen, 1982; Meyer and Okamura, 1985; Vecchio and Collins, 1986; Pfeiffer et al., 1990; Hu and Schnobrich, 1991; Borri and Sorace, 1993). Nowadays, the ultimate pressure capability of the nuclear reactor containment can be predicted more accurately than before by utilizing the nonlinear finite element method (Pfeiffer et al., 1992; Andreoli et al., 1993; Saito et al., 1993). The Atomic Energy Council (AEC) at Taiwan, ROC is currently running several studies toward the failure analysis of containment structures. As one of the research projects sponsored by AEC, the

* Corresponding author. Tel.: +886-6-2757575 ext 63168; fax: +886-6-2358542.

*E-mail address:* hthu@mail.ncku.edu.tw (H.-T. Hu)

0029-5493/00/$ - see front matter 
PII: S0029-5493(99)00163-6

aim of this paper is to employ the nonlinear finite element program ABAQUS (Hibbitt et al., 1997) to investigate the ultimate pressure capacity and the failure mode of the BWR Mark III reinforced concrete containment at Kuosheng nuclear power plant, Taiwan, ROC.

In the paper, the geometry and finite element mesh of the containment are reviewed first. Then, material properties of reinforcing steel, liner plate and concrete are given and proper constitutive models are introduced to simulate the nonlinear behavior of these materials such as concrete cracking, tension stiffening, shear retention, concrete plasticity, yielding of reinforcing steel, yielding of liner plate and degradation of material properties because of high temperature effects. Finally, failure analyses of the containment subjected to internal pressure are carried out and important conclusions are given.

## 2. Containment geometry and finite element mesh

The BWR reinforced concrete containment at Kuosheng Nuclear Power Plant is composed of a circular base slab, an upright cylinder and a hemispherical dome (Fig. 1). To simplify the analysis, equipment hatches and penetrations on the containment are not considered and the structure geometry is assumed to be axisymmetric. The top of the containment is about 220′ above ground. The inner radius of the dome is 62′. The thickness of the dome varies from 2′–6″ at the apex to 3′–6″ at the spring line. The inner diameters of the upper cylinder and the lower cylinder are 124′ and 114′. The thicknesses of the upper cylinder and the lower cylinder are 3′–6″ and 8′–6″, respectively. The base slab is made of a 10′–6″ thick flat circular plate with a diameter of 141′.

The entire interior surface of the dome, cylinder and base slab are lined with continuous steel plate system to provide a leak-tight barrier. The thickness of the steel liner plate inside the dome and cylinder is 1/4″ while the thickness of the steel plate on the base slab is 2″. Most of the steel reinforcing bars are placed in an axisymmetric manner in the containment and the detailed arrangements of steel reinforcing bars are given in the Final Safety Analysis Report of the Kuosheng nuclear power plant (Taiwan Power Company, 1979). Because some steel reinforcement layers in the base slab are placed in the directions parallel to x and y axes, the deformation of the containment will no longer be axisymmetric and will have four planes of symmetry (Fig. 2a). As a result, only 1/8 part of the structure is analyzed and the boundary conditions imposing on the symmetric planes are displacements in the circumferential direction, rotations in the radial direction and rotations in the z direction to be zero. In the numerical simulation, 8-node shell elements (six degrees of freedom per node) are used to model the parts of dome and cylinder, and 27-node solid elements (three degrees of freedom per node) are used to model the base slab (Fig. 2b). The liner plates are also modeled by the 8-node shell elements. They are either linked to the shell elements of the concrete section (without any offset) at the parts of dome and cylinder, or attached to the inner surface of the solid elements at the base

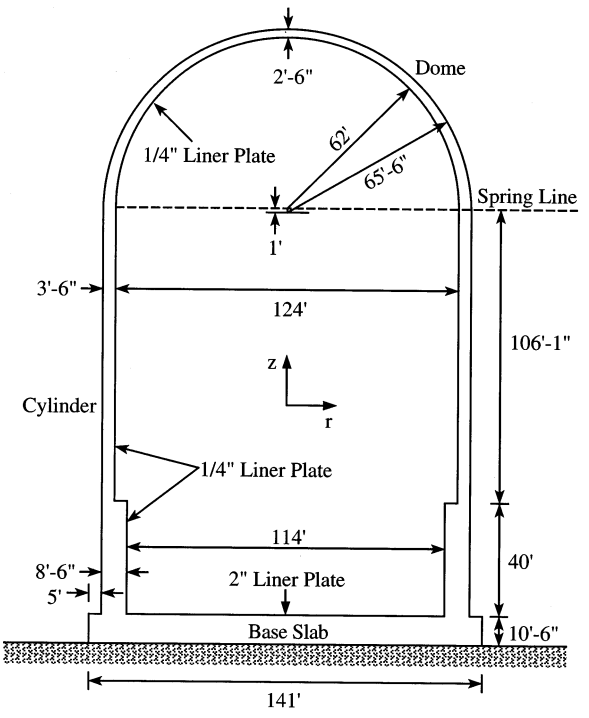


Fig. 1. Geometry and dimensions of the BWR reinforced concrete containment of Kuosheng nuclear power plant.

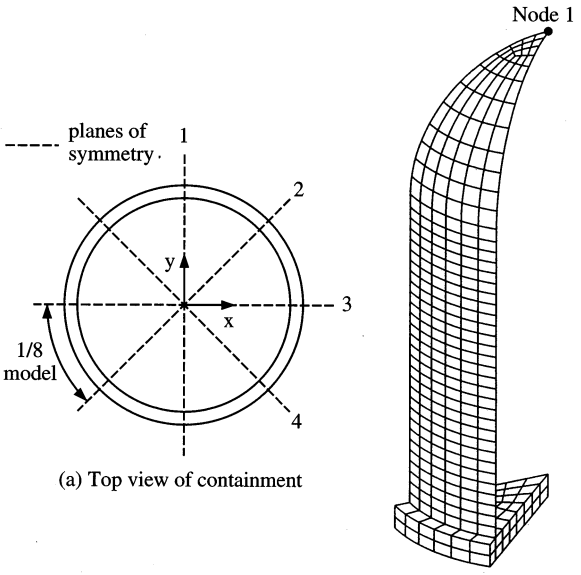


Fig. 2. 1/8 model of the BWR Mark III reinforced concrete containment of Kuosheng nuclear power plant.

slab. The formulation of the 8-node shell allows transverse shear deformation and these shear flexible shell elements can be used for both thick and thin shell analysis (Hibbitt et al., 1997). At the bottom of the base slab, special purpose 9-node interface elements are used to link the base slab to the ground. The interface elements allow the contact surfaces between the base slab and the ground to remain closed or open but not to penetrate each other.

## 3. Material properties and constitutive models

The materials used in the containment can be divided into three groups, which are steel reinforcing bar, steel liner plate and concrete. The material properties of all the materials and their constitutive models used by ABAQUS are briefly discussed in the following sections.

### 3.1. Steel reinforcing bar

The reinforcement used in the containment structure is ASTM A-615 Grade 60 steel with yielding stress

$$\sigma_y = 60 \text{ ksi} \quad (1)$$

and its elastic modulus is assumed to be

$$E_S = 29\,000 \text{ ksi} \quad (2)$$

The stress-strain curve of the reinforcing bar is assumed to be elastic perfectly plastic as shown in Fig. 3. In ABAQUS, the steel reinforcement is treated as an equivalent uniaxial material, which is smeared through the element section. In order to properly model the constitutive behavior of the reinforcement, the cross sectional area, spacing, position and orientation of each layer of steel bar within each element need to be specified.

### 3.2. Steel liner plate

The 1/4″ liner plate inside the dome and cylinder is ASTM SA-285 Grade A or C carbon steel with yield stress

$$\sigma_y = 24 \text{ ksi} \quad (3)$$

The 2″ liner plate on the base slab is ASTM SA-516 Grade 70 stainless steel with yield stress

$$\sigma_y = 38 \text{ ksi} \quad (4)$$

In the analysis, the elastic modulus $E_S$ and the Poisson's ratio $v_S$ of both types of steel liner plates are assumed to be

$$E_S = 29\,000 \text{ ksi} \quad (5)$$

$$v_S = 0.3 \quad (6)$$

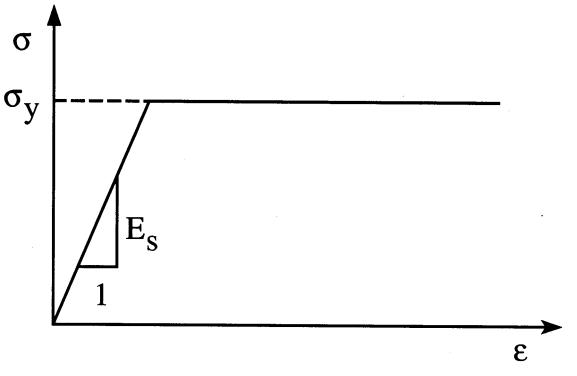


Fig. 3. Elastic perfectly plastic model for steel reinforcing bar and steel liner plate.

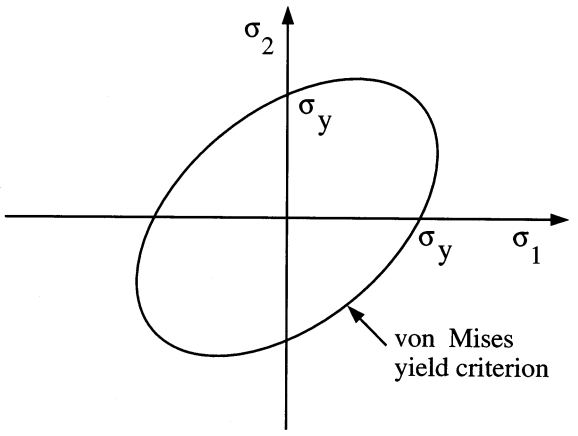


Fig. 4. Von Mises yield criterion for steel liner plate.

The uniaxial behavior of the steel liner plate is similar to reinforcing bar and thus can be simulated by an elastic perfectly plastic model as shown in Fig. 3. When the liner plate is subjected to biaxial stresses, a von Mises yield criterion $f(\sigma_1,\sigma_2)$ is employed to define the elastic limit (Fig. 4), where $\sigma_1$ and $\sigma_2$ are principal stresses and

$$f(\sigma_1, \sigma_2) = \sqrt{\sigma_1^2 + \sigma_1^2 - \sigma_1\sigma_2} = \sigma_y$$
$$(\sigma_y = \text{yield stress}) \quad (7)$$

The response of the liner plate is modeled by an elastic-perfectly plastic theory with associated flow rule. When the stress points fall inside the yield surface, the behavior of the liner plate is linearly elastic. If the stresses of the liner plate reach the yield surface, the behavior of the liner plate becomes perfectly plastic. Consequently, the liner plate is assumed to fail and can not resist any further loading.

### 3.3. Concrete

The concrete used in the containment structure has an uniaxial compressive strength $f'_c$ given as

$$f'_c = 5000 \text{ psi} \quad (8)$$

Under uniaxial compression, the concrete strain $\varepsilon_o$ corresponding to the peak stress $f'_c$ is usually around the range of 0.002 to 0.003. A representative value suggested by ACI Committee 318 (1995) is

$$\varepsilon_o = 0.003 \quad (9)$$

The Poisson's ratio $v_c$ of concrete under uniaxial compressive stress ranges from about 0.15 to 0.22, with a representative value of 0.19 or 0.20 (ASCE, 1982). In this study, the Poisson's ratio of concrete is assumed to be

$$v_c = 0.2 \quad (10)$$

The uniaxial tensile strength $f'_t$ of concrete is difficult to measure and is normally taken as approximately (ASCE, 1982)

$$F'_t = 4\sqrt{f'_c} \text{ psi} \quad (11)$$

The initial modulus of elasticity of concrete $E_c$ is highly correlated to its compressive strength and can be calculated with reasonable accuracy from the empirical equations (ACI Committee 318, 1995)

$$E_c = 57\,000\sqrt{f'_c} \text{ psi} \quad (12)$$

Under different combinations of loading, the failure strengths of concrete are different from that under uniaxial condition. However, the maximum strength envelope under multiple stress conditions seems to be largely independent of load path (Kupfer et al., 1969; Nelissen, 1972). In ABAQUS, a Mohr–Coulomb type compression surface combined with a crack detection surface are used to model the failure surface of concrete (Fig. 5). When the principal stress components of concrete are predominantly compressive, the response of the concrete is modeled by an elastic-plastic theory with associated flow and isotropic hardening rule. In tension, once cracking is defined to occur (by the crack detection surface), the orientation of the cracks is stored, and oriented. Damaged elasticity is then used to model the existing cracks.

When plastic deformation occurs, there should be a certain parameter to guide the expansion of the yield surface. A commonly used approach is to relate the multidimensional stress and strain conditions to a pair of quantities, namely, the effective stress $\sigma_c$ and effective strain $\varepsilon_c$, such that results obtained following different loading paths can all be correlated by means of the equivalent uniaxial stress-strain curve. The stress-strain rela-

tionship proposed by Saenz (1964) has been widely adopted as the uniaxial stress-strain curve for concrete and it has the following form

$$\frac{E_c\varepsilon_c}{1+(R+R_E-2)\left(\frac{\varepsilon_c}{\varepsilon_o}\right)-(2R-1)\left(\frac{\varepsilon_c}{\varepsilon_o}\right)^2+R\left(\frac{\varepsilon_c}{\varepsilon_o}\right)^3} \tag{13}$$

where $R=\frac{R_E(R_\sigma-1)}{(R_\varepsilon-1)^2}-\frac{1}{R_\varepsilon}$, $R_E=\frac{E_c}{E_o}$, $E_o=\frac{f'_c}{\varepsilon_o}$ and $R_\sigma=4$, $R_\varepsilon=4$ may be used (Hu and Schnobrich, 1991). In the analysis, Eq. (13) is taken as the equivalent uniaxial stress-strain curve for concrete and approximated by several piecewise linear segments as shown in Fig. 6.

When cracking of concrete takes place, a smeared model is used to represent the discontinuous macrocrack behavior. It is known that the cracked concrete of a reinforced concrete element can still carry some tensile stress in the direction normal to the crack, which is termed tension stiffening (ASCE, 1982). In this study, a simple descending line is used to model this tension stiffening phenomenon (Fig. 7). The default value (Hibbitt et al., 1997) of the strain $\varepsilon^*$ at which the tension stiffening stress reduced to zero is

$$\varepsilon^*=0.001 \tag{14}$$

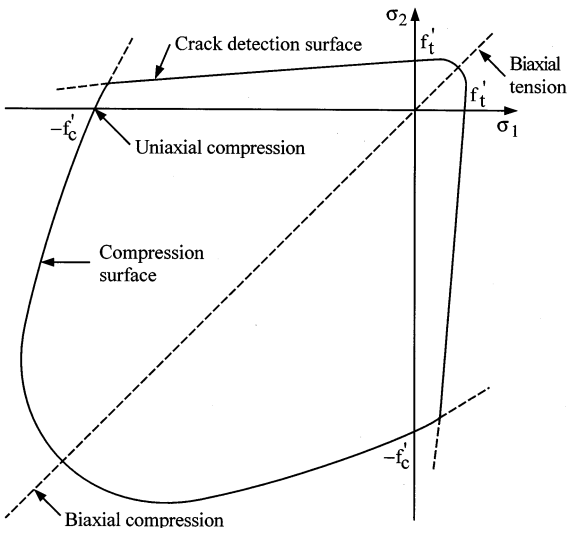


Fig. 5. Concrete failure surface in plane stress.

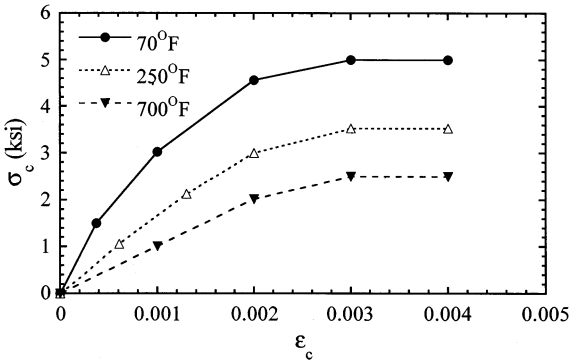


Fig. 6. Equivalent uniaxial stress-strain curves for concrete under different temperature conditions.

During the postcracking stage, the cracked reinforced concrete can still transfer shear forces through aggregate interlock or shear friction, which is termed shear retention. Assuming that the shear modulus of intact concrete is $G_c$, then the reduced shear modulus $\hat{G}$ of cracked concrete can be expressed as

$$\hat{G}=\mu G_c \tag{15a}$$

and

$$\mu=1-\varepsilon/\varepsilon_{max} \tag{15b}$$

where $\varepsilon$ is the strain normal to the crack direction and $\varepsilon_{max}$ is the strain at which the parameter $\mu$ reduces to zero (Fig. 8). In ABAQUS, $\varepsilon_{max}$ is usually assumed to be a very large value, i.e. $\mu=1$ (full shear retention). In this investigation, other than specified, the default values for tension stiffening parameter $\varepsilon^*=0.001$ and for shear retention parameter $\mu=1$ are used.

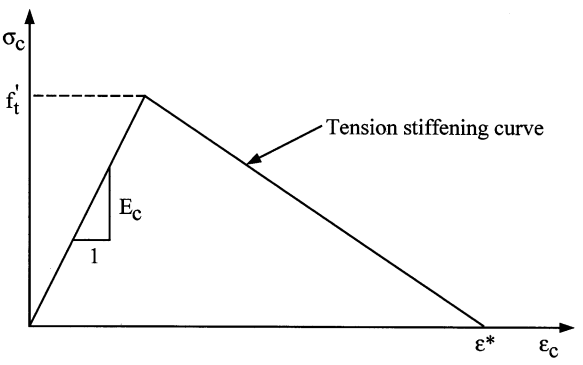


Fig. 7. Tension stiffening model.

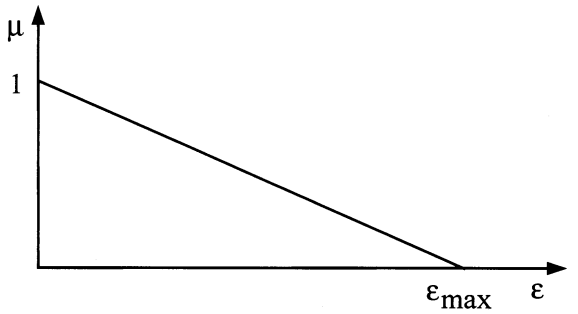


Fig. 8. Shear retention parameter.

### 3.4. Material properties at elevated temperature

All the aforementioned material properties for steel and concrete are tested or assumed under the room temperature condition. In the case of a nuclear accident, the containment will usually be subjected to elevated temperature and internal pressure and the degradation of material properties as a result of high temperature effects should be considered. Owing to the material properties of Kuosheng Nuclear Power Plant at elevated temperatures being unavailable, the ratios of material properties at elevated temperature to those at room temperature as given in Table 1 (Pfeiffer et al., 1990) are used to linearly scale down the material properties in the high temperature analyses. The material properties used in analysis in the room temperature (70°F) condition and at elevated temperature (250°F and 700°F) conditions are given in Table 2. The equivalent uniaxial stress-strain curves for concrete at different temperatures are shown in Fig. 6. In this paper, other than specified, all the analyses are assumed to be carried out at the room temperature (70°F) condition.

Table 1
Material properties for concrete and steel at various temperatures (Pfeiffer et al., 1990)

| | Temperatures | | |
|---|---|---|---|
| | 70 (°F) | 250 (°F) | 700 (°F) |
| *Concrete* | | | |
| Young's modulus $E_c$ (ksi) | 4800 | 2300 | 1200 |
| Poisson's ratio $v_c$ | 0.2 | 0.2 | 0.2 |
| Tensile strength $f'_t$ (psi) | 500 | 353 | 250 |
| Compressive strength $f'_c$ (psi) | 6800 | 4800 | 3400 |
| *Steel* | | | |
| Young's modulus $E_s$ (ksi) | 31 000 | 28 500 | 25 700 |
| Poisson's ratio $v_s$ | 0.3 | 0.3 | 0.3 |
| Yield stress $\sigma_y$ (ksi) | 66.6 | 56.6 | 51.3 |

## 4. Numerical analysis

### 4.1. Influence of containment dead load on the ultimate pressure capacity of the containment

The containment structure has a considerable amount of dead load contributed by reinforced concrete. It is interesting to study the influence of this dead load on the ultimate pressure capacity of the containment. In this investigation, it is assumed that the dead load, $w_c$, caused by the reinforced concrete (Wang and Salmon, 1998) is

$$w_c = 150 \text{ lb/ft}^3 \tag{16}$$

Fig. 9 shows the internal pressure p verse the displacement of node 1 (at the apex of the containment) in z direction. When the dead load and steel liner plate are considered in the analysis, the ultimate internal pressure $p_u$ of the containment is 23.9 psi, which is about 59% higher than the design pressure 15 psi (Taiwan Power Company, 1979). The deformation shape of the containment under the ultimate internal pressure condition is shown in Fig. 10a and the crack patterns of the concrete at the inner and outer sides of containment are shown in Fig. 11. From these figures we can observe that under the ultimate pressure, the base slab still keeps in contact with the ground. Most of the deformations take place in the upper cylinder and dome. In addition, because of stress concentration, cracks are likely to occur near the apex of the dome, the conjunction of dome and cylinder, and the mid-cylinder location where the thickness changes abruptly (Fig. 1).

Table 2
Material properties used for BWR Mark III reinforced concrete containment in numerical analysis

| | Temperatures | | |
|---|---|---|---|
| | 70 (°F) | 250 (°F) | 700 (°F) |
| *Concrete* | | | |
| Young's modulus $E_c$ (ksi) | 4031 | 1931 | 1008 |
| Poisson's ratio $v_c$ | 0.2 | 0.2 | 0.2 |
| Tensile strength $f'_t$(psi) | 282.8 | 199.7 | 141.4 |
| Compressive strength $f'_c$ (psi) | 5000 | 3529 | 2500 |
| Strain at compressive strength $\varepsilon_o$ | $3\times10^{-3}$ | $3\times10^{-3}$ | $3\times10^{-3}$ |
| Tension stiffening parameter $\varepsilon$* | $1\times10^{-3}$ | $1\times10^{-3}$ | $1\times10^{-3}$ |
| Shear retention parameter $\mu$ | 1 | 1 | 1 |
| *Steel* | | | |
| Young's modulus $E_s$ (ksi) | 29 000 | 27 700 | 24 700 |
| Poisson's ratio $v_s$ | 0.3 | 0.3 | 0.3 |
| [a]Yield stress $\sigma_y$ (ksi) | 60 | 55.0 | 47.4 |
| [b]Yield stress $\sigma_y$ (ksi) | 24 | 21.0 | 19.0 |
| [c]Yield stress $\sigma_y$ (ksi) | 38 | 34.8 | 30.0 |

[a] Reinforcing bar.
[b] 1/4″ liner plate.
[c] 2″ liner plate.

With the dead load of the reinforced concrete being neglected and with the liner plate being considered, the ultimate pressure capacity of the containment significantly reduces to 10 psi (Fig. 9), which is about 33% lower than the design pressure. This is because, when the dead load of the reinforced concrete is neglected, the base slab tends to uplift and is consequently subjected to too much bending (Fig. 10b). While the dome and cylindrical parts of the containment are still intact, major cracks take place at the bottom and center of the base slab and the structure fails at very low internal pressure. From these analyses, we can see that the dead load behaves like a prestress acting on the containment and strengthens the containment significantly. If the dead load of the reinforced concrete is not included in the ultimate analysis of the containment, this will lead to an incorrect failure mode.

### 4.2. Influence of liner plate on the ultimate pressure capacity of the containment

The capability of the liner plate to support the containment in resisting the internal pressure is investigated in this section. From Fig. 9 we can find that with the dead load of the reinforced concrete being considered and with liner plate being neglected, the ultimate pressure capacity of the containment is 17.9 psi, which is a 25% reduction in the ultimate pressure capacity. Hence, it is important to incorporate the steel liner plate in the ultimate analysis.

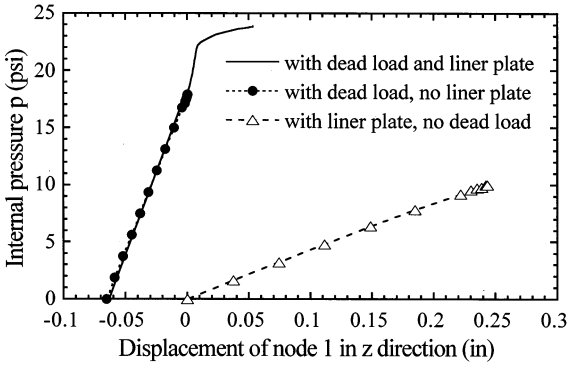


Fig. 9. Influence of dead load and liner plate on the ultimate pressure capacity of containment.

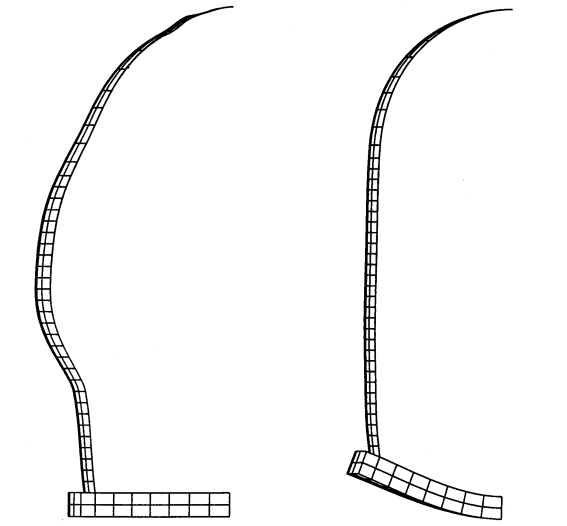


Fig. 10. Deformation shapes (side view) of containment at the ultimate internal pressure.

### 4.3. Influence of geometric nonlinearity on the ultimate analysis

Fig. 12 shows the load-displacement curves of node 1 by considering different combinations of material nonlinearity and geometric nonlinearity. When all the materials of the containment, i.e. concrete, steel reinforcing bars and steel liner plate, have a linear elastic behavior, the result of analysis by employing the geometric nonlinear formulation is almost the same as that by using the geometric linear formulation. It can then be concluded that when the containment fails, the deformation of the containment is still small and the geometric nonlinear effect is negligible.

### 4.4. Influence of tension stiffening on the ultimate pressure capacity of the containment

Fig. 13 shows the load-displacement curves of node 1 obtained by varying the tension stiffening parameter $\varepsilon^*$ (Fig. 7). When $\varepsilon^*$ is set to a very small value close to the crack strain $\varepsilon_{cr} = f'_t/E_c$ of concrete, i.e. no tension stiffening, the ultimate pressure capacity of containment is 17.4 psi, which should be the lower bound of the ultimate pressure. When the tension stiffening phenomenon is considered, the resulting ultimate pressures of the containment are very close. Although, $\varepsilon^*$ is increased 10 times from 0.001 (default) to 0.01, the deviation of the ultimate pressure is less than 3%. Hence, as long as tension stiffening is properly taken into consideration, the influence of the tension stiffening parameter on the ultimate pressure capacity of containment may not be significant.

### 4.5. Influence of shear retention on the ultimate pressure capacity of the containment

Fig. 14 shows the load-displacement curves of node 1 obtained by using full shear retention and

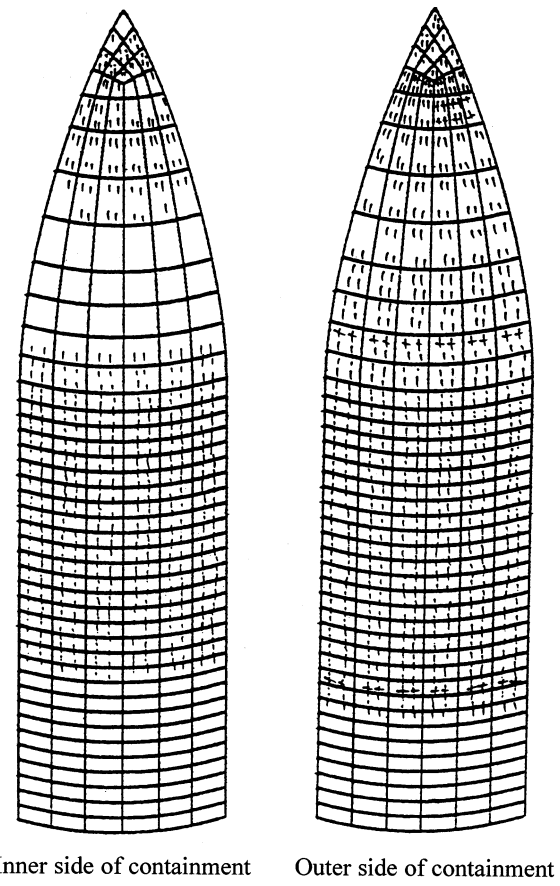


Fig. 11. Crack pattern of containment at the ultimate internal pressure $p_u = 23.9$ psi (with dead load and liner plate).

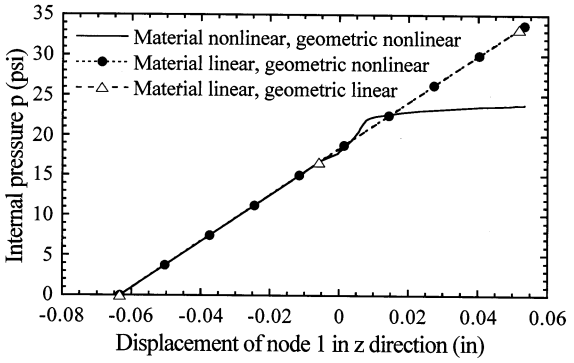


Fig. 12. Influence of geometric nonlinearity on the ultimate analysis.

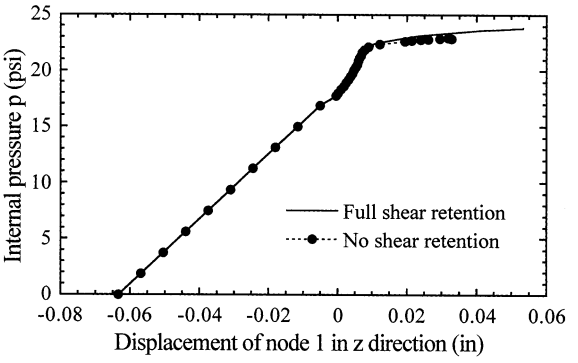


Fig. 14. Influence of shear retention on the ultimate pressure capacity of containment.

no shear retention. For full shear retention, the parameter $\mu$ is selected to be 1 (Fig. 8), and the shear modulus of cracked concrete is assumed to be the same as that of intact concrete. For no shear retention, the parameter $\mu$ is selected to be 0, and the shear modulus of cracked concrete is assumed to be zero. From the figure we can see that the load-displacement curves of these two extreme conditions are very close and similar. In addition, the difference of the ultimate pressure capacity for these two cases is small and within 4%. Hence, it can be concluded that shear retention has very little influence on the ultimate pressure capacity of containment. It could be because of the fact the model is quasi axisymmetric and then without shear effects.

### *4.6. Influence of base slab on the ultimate pressure capacity of the containment*

In previous sections, the containment in numerical analysis includes dome, cylinder and base slab. From Fig. 10a and Fig. 11 we can observe that under the ultimate internal pressure condition, major cracks occur at the dome and cylinder. As a result of the dead load effect, the base slab has very little deformation. Hence, for the sake of saving computer time, it may be interesting to perform the finite element analysis again without the base slab and assume the cylinder to be clamped to the ground directly. Fig. 15 shows the load-displacement curves of the containment

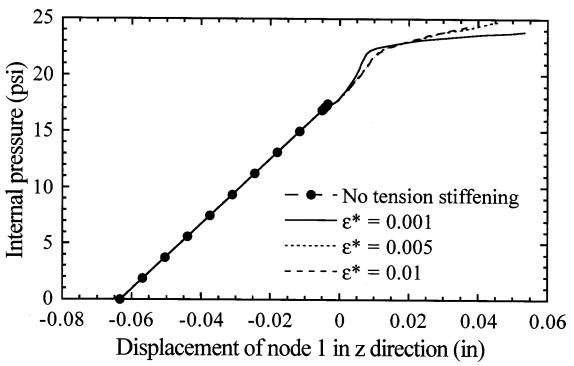


Fig. 13. Influence of tension stiffening on the ultimate pressure capacity of containment.

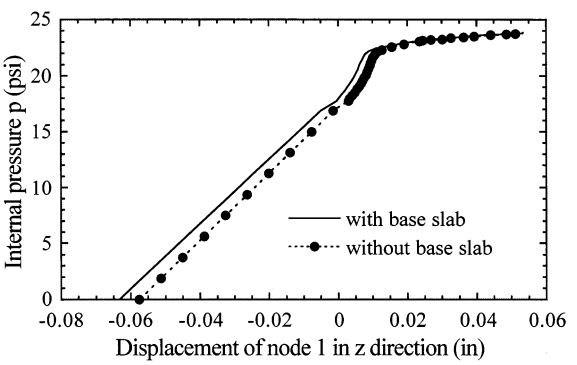


Fig. 15. Influence of base slab on the ultimate pressure capacity of containment.

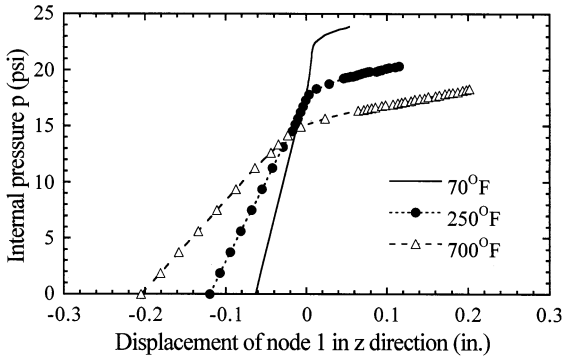


Fig. 16. Influence of temperature on the ultimate pressure capacity of containment.

with and without base slab. It can be observed that these two curves are very close and the ultimate pressure capacity for these two analyses are almost the same (0.5% difference). In addition, under the ultimate pressure condition, the crack patterns for these two analyses are also very similar (Liang, 1996).

### *4.7. Influence of temperature on the ultimate pressure capacity of the containment*

In this section, numerical analyses are carried out at the elevated temperature conditions (250°F and 700°F). For the sake of simplicity, heat transfer studies are not performed. The entire containment is assumed to be subjected to the same elevated temperature and thermal stresses introduced as a result of the temperature change are neglected. In the analyses, the degraded material properties given in Table 2 are used. Fig. 16 shows that the ultimate pressure capacity of the containment is 20.3 psi under 250°F temperature and is 18.3 psi under 700°F temperature conditions. In addition, the stiffness of the containment is reduced with increasing temperature. From Tables 1 and 2, we can find that the degradation of the ultimate pressure capacity and the stiffness of the containment is primarily a result of the weakening of the concrete. Nevertheless, the ultimate pressure capacity of the containment under 700°F temperature condition is still higher than the design load of 15 psi by 22%.

## 5. Conclusions

In this paper, nonlinear finite element analyses of the BWR Mark III reinforced concrete containment at Kuosheng nuclear power plant are performed. For simplicity, equipment hatches and penetrations on the containment are not considered. Based on the numerical results from the analyses, the following conclusions may be drawn:

1. The ultimate pressure capacity of the containment is 23.9 psi, which is about 59% higher than the design pressure. Under the ultimate pressure condition, cracks are likely to occur near the apex of the dome, the conjunction of dome and cylinder, and the mid-cylinder location where the thickness changes abruptly.
2. The dead load of the reinforced concrete behaves like a prestress load acting on the containment and strengthens the containment significantly. If the dead load of the reinforced concrete is not included in the ultimate analysis of the containment, this will lead to an incorrect failure mode. In addition, it is also important to incorporate the steel liner plate in the ultimate analysis.
3. When the containment fails, the deformation of the containment is still small and the geometric nonlinear effect is negligible.
4. As long as tension stiffening is properly taken into consideration, the influence of the tension stiffening parameter on the ultimate pressure capacity of the containment may not be significant.
5. Shear retention has very little influence on the ultimate pressure capacity of the containment.
6. For the sake of saving computer time, the base slab may be excluded from the ultimate analysis of the containment and the cylinder part of the containment can be assumed to be clamped to the ground directly.
7. The ultimate pressure capacity and the stiffness of the containment are significantly influenced by elevated temperature. However, the ultimate pressure capacity of the containment under a temperature of 700°F is still higher than the design load.

## Acknowledgements

This research work was financially supported by the Atomic Energy Council of the Republic of China under Grant 852001NRD002.

## References

ASCE Task Committee on Concrete and Masonry Structure, State of the Art Report on Finite Element Analysis of Reinforced Concrete, ASCE, New York, 1982.

ACI Committee 318, Building Code Requirements for Structural Concrete (ACI 318-95), American Concrete Institute, Detroit, Michigan, 1995.

Amin, M., Eberhardt, A.C., Erler, B.A., 1993. Design considerations for concrete containments under severe accident loads. Nucl. Eng. Des. 145, 331–338.

Andreoli, V., Angeloni, P., Contri, P., Brusa, L., 1993. Numerical simulation of the ultimate capacity of a reactor containment building. Nucl. Eng. Des. 145, 403–417.

Boeck, B.D., 1993. A review of containment accidents. Nucl. Eng. Des. 145, 279–288.

Borri, A., Sorace, S., 1993. FE analysis strategies for structural materials with small tensile strength. J. Press. Vessel Technol. 115, 156–163.

Chen, W.F., 1982. Plasticity in Reinforced Concrete. McGraw-Hill, New York.

Hibbitt, Karlsson and Sorensen, Inc., ABAQUS Theory Manual and User Manual, Version 5.5, Providence, Rhode Island, 1997.

Hu, H.-T., Schnobrich, W.C., 1991. Nonlinear finite element analysis of reinforced concrete plates and shells under monotonic loading. Comput. Struct. 38, 637–651.

Kupfer, H., Hilsdorf, H.K., Rusch, H., 1969. Behavior of concrete under biaxial stresses. ACI J. 66, 656–666.

J.-I. Liang, Analysis of the Ultimate Pressure Capacity for the Reinforced Concrete Containment of Kuosheng Nuclear Power Plant, M.S. Thesis, Department of Civil Engineering, National Cheng Kung University, Tainan, Taiwan, ROC, 1996.

Meyer, C., Okamura, H., 1985. Finite Element Analysis of Reinforced Concrete Structures. ASCE, New York.

Nelissen, L.J.M., 1972. Biaxial testing of normal concrete. Heron 18, 1–90.

U.S. Nuclear Regulatory Commission, Office of Nuclear Reactor Regulation, Standard Review Plan for the Review of Safety Analysis Reports for Nuclear Plants, Section 3.8.1, NUREG-0800, June 1987.

Pfeiffer, P.A., Kennedy, J.M., Marchertas, A.H., 1990. Thermal effects in the overpressurization response of reinforced concrete containment. Nucl. Eng. Des. 120, 25–34.

Pfeiffer, P.A., Kennedy, J.M., Marchertas, A.H., 1992. Post-test analysis for the nonlinear response of an internally pressurized one sixth scale reinforced concrete containment model. Nucl. Eng. Des. 133, 143–157.

Saito, H., Muramatsu, Y., Furukawa, H., Hasegawa, T., Mutoh, A., 1993. Post-test analysis of a 1:10-scale top slab model of ABWR/RCCV subjected to internal pressure. Nucl. Eng. Des. 145, 339–353.

L.P. Saenz, Discussion of 'Equation for the Stress-Strain Curve of Concrete,' by P. Desayi and S. Krishnan, ACI Journal 61 (1964) 1229-1235.

Taiwan Power Company Final Safety Analysis Report, Kuosheng Nuclear Power Station Units 1 and 2, Volume 5, 1979.

Vecchio, F.J., Collins, M.P., 1986. The modified compression-field theory for reinforced concrete elements subjected to shear. ACI J. 83, 219–231.

Wang, C.-K., Salmon, C.G., 1998. Reinforced Concrete Design, Chapter One, Sixth Edition. Addison Wesley, New York.